

Journal of Mechanics of Materials and Structures

NONLINEAR CREEP RESPONSE
OF REINFORCED CONCRETE BEAMS

Ehab Hamed

Volume 7, No. 5

May 2012

NONLINEAR CREEP RESPONSE OF REINFORCED CONCRETE BEAMS

EHAB HAMED

The nonlinear viscoelastic behavior of reinforced concrete beams under sustained loading is investigated in this paper. A theoretical model is developed, which is based on the viscoelastic modified principle of superposition, and accounts for cracking, nonlinear behavior in compression, shrinkage, aging, and the creep rupture phenomenon of concrete. A nonlinear form of the relaxation modulus is presented, which is introduced into the constitutive relations and the corresponding nonlinear rheological Maxwell model, to account for damage. The governing equations are solved through time-stepping numerical integration, which yields an exponential algorithm following the expansion of the relaxation modulus into a Dirichlet series. The determination of the section-equivalent rigidities and creep strains along the cracked and uncracked regions is achieved through an iterative procedure at each time step. The capabilities of the model are demonstrated through numerical examples and parametric studies including comparison with test results available in the literature. The results show that creep has various and different influences on the structural response, and in some cases it may lead to a reduction of the load-carrying capacity of the member by creep rupture-type of failures.

1. Introduction

The creep behavior of reinforced concrete (RC) members in general and RC beams in particular has been intensively studied. Normally, the long-term effects of creep and shrinkage lead to a progressive increase in the deformations and a change of the cracking pattern over time, which are assumed to only affect the serviceability of RC members. Nevertheless, in some cases, structural members may be subjected to high levels of sustained loads, as is the case with dams, retaining walls, beam-columns, arches, containment vessels, cooling towers, and others. In such cases, the creep and shrinkage effects may put the structure out of service, may reduce the residual load-carrying capacity of the member over time (and hence reduce the factor of safety for failure), or may even lead to premature failures. This paper deals with the nonlinear viscoelastic behavior of RC members including the phenomenon of creep rupture, with special focus on RC beams.

The nonlinear viscoelastic response of RC beams exhibits a number of physical phenomena that require special attention. Among those is the time-dependent variation of the internal stresses with time, which results from the linear brittle behavior of concrete in tension and the nonlinear behavior in compression, and also from the restraint of the long-term effects by the steel reinforcement. This stress redistribution is combined with the shifting of the neutral axis with time. The prediction of these two effects becomes very

The work reported in this paper was supported by the Australian Research Council (ARC) through a Discovery Project (DP0987939).

Keywords: cracking, creep, long-term, nonlinear, reinforced concrete, viscoelasticity.

challenging under high levels of sustained loads due to the nonlinearity of stresses and their influence on the creep response, which cannot be described using the well-known linear viscoelastic models [Neville and Dilger 1970; Gilbert 1988]. Another phenomenon that results from the long-term effects is the propagation and widening of flexural cracks with time, as a result of the combined effects of creep, restrained shrinkage, and creep rupture in tension, in which the tensile capacity of concrete decreases over time. As a result of the latter effect, long-term cracking of points that are under sustained tensile stresses greater than about 70% of the tensile strength may occur [Zhou 1994]. Similar response occurs also in compression, where creep rupture of material points under sustained stress that is greater than about 80% of the compressive strength may occur [Carol and Murcia 1989; CEB-FIP 1990; Mazzotti and Savoia 2003], reducing the load-carrying capacity and the factor of safety of RC flexural members. Some experimental results regarding creep rupture in flexural plain concrete beams with notches were reported in [Omar et al. 2009], and it was revealed that tertiary creep and rupture occurred at load levels greater than 70% of the maximum load-carrying capacity. Understanding and clarifying these aspects, as well as the development of suitable and reliable theoretical models for their prediction, are essential for the safety assessment of existing structures and the design of new ones.

Bažant and Asghari [1977] combined the endochronic theory with a linear Maxwell chain model for investigating the nonlinear creep response of plain concrete under compression, but without considering the behavior of flexural members. In another study, Bažant and Chern [1985] developed a model suitable for finite element analysis of plain concrete using a strain softening element connected in series to a generalized Maxwell chain that describes the uncracked response. Yet, the response of RC flexural members and the incorporation of the material nonlinearity in compression were not considered. Papa et al. [1998] proposed an approach to model the progressive microcracking and creep acceleration of plain concrete under tension and compression, by gradually varying the Maxwell constants based on a damage variable. Mazzotti and Savoia [2003] combined the solidification theory of [Bažant and Prasannan 1989] with a damage model for the description of the nonlinear creep response of plain concrete under compression. Fernández Ruiz et al. [2007] proposed a simplified plasticity-damage model for plain concrete under compression. The nonlinear relation between creep strains and the stress level was introduced in their study through a stress-dependent creep coefficient (see also [CEB-FIP 1990]).

The studies mentioned above and many others [Carol and Murcia 1989; Santhikumar et al. 1998; Di Luzio 2009] focused on the creep response of plain concrete, while the nonlinear creep behavior of RC members has received less attention. The only studies that could be found in the literature regarding the nonlinear creep response of RC beams are those of [Bažant and Oh 1984; Li and Qian 1989]. The former was based on the effective elastic modulus approach and the linear principle of superposition, which are more appropriate for linear material response, and it did not include the effects of creep rupture and shrinkage-induced deformations. The latter included only a section analysis based on a creep damage model that depends on a number of parameters determined empirically. Limited results that include the time variation of the curvature were presented in [Li and Qian 1989], without the description of stresses, their relaxation and redistribution with time, propagation of cracking, creep rupture, and other effects.

In this paper, the nonlinear viscoelastic response of RC beams is investigated through a full nonlinear viscoelastic model that is based on the modified principle of superposition [Leaderman 1943]. This modeling approach also provides a potential alternative to most existing nonlinear creep models for plain concrete, which are based on combinations of linear viscoelastic rheological models with nonlinear

sliders, to model either cracking or material softening. The single-integral nonlinear viscoelastic model used here is converted into a differential-type relation after the expansion of the nonlinear relaxation modulus into a Dirichlet series. This yields a nonlinear generalized Maxwell model with the damage being modeled as strain-dependent spring and dashpot constants. The model uses beam theory with first-order shear deformations (Timoshenko beam), and it accounts for creep rupture under both tension and compression, shrinkage, aging, and yielding of the steel reinforcement, through an incremental time-stepping analysis. The mathematical model is applicable for any stress loading history, and any geometry, boundary conditions, and material properties. The assumptions made in the material and structural modeling are included in the mathematical formulation, which is followed by a numerical study and a comparison of the proposed model with experimental results.

2. Mathematical formulation

The mathematical formulation presented here focuses on RC beams, but it provides a basis for modeling further related structural members. The constitutive relations at the concrete material level and at the section level are presented first. They are followed by the formulation of the governing incremental equations and a description of the solution procedure. A smeared cracking modeling approach with full bonding between the concrete and the steel reinforcement is adopted, along with a distinction between the cracked and uncracked regions along the beam. It has been shown in many research studies [Rots and Blaauwendraad 1989] that the smeared cracking model, which assumes that stresses and strains are averaged over a representative length to span several cracks and microcracks, is an effective approach for predicting the cracking and post-cracking response of RC flexural members. This is mainly because it describes an integrated effect of the localized flexural cracks and microcracks, which are characterized by some levels of uncertainty regarding their real distribution. There is no doubt, however, that a discrete cracking model with a bond-slip law between the concrete and the steel will present a more comprehensive and accurate description of the localized structural behavior, but this effect is not described here. The sign conventions for the coordinates, deformations, loads, stresses, and stress resultants of a typical RC beam appear in Figure 1.

2.1. Constitutive relations at the material level. The constitutive relations are assumed to be independent of temperature and other environmental effects in order to clarify and highlight the time-dependent effects of creep and shrinkage. A superposition between the nonlinear viscoelastic strain ε_{xx}^v (equal to the instantaneous strain ε_{xx}^{ins} plus the creep strain ε_{xx}^{cp}) and the stress-independent shrinkage strain ε_{sh} is assumed, that is, $\varepsilon_{xx} = \varepsilon_{xx}^v + \varepsilon_{sh}$, with ε_{xx} being the total strain. The instantaneous strain is related to the applied stress via a nonlinear short-term constitutive relation that accounts for cracking and material softening in compression, and it can refer to the elastic, inelastic, or cracking strains. The short-term constitutive relation provides the basis for developing the nonlinear relaxation function (as discussed in Section 3.1), which is used in the nonlinear viscoelastic model to describe the effects of cracking and damage produced by the creep strain as well. The formulation presented here is used to describe the creep and the short-term response; whereas the latter is obtained by choosing a number of fairly small time steps between $t = 10^{-9}$ to $t = 10^{-8}$ days, for example.

As mentioned earlier, the modified principle of superposition is adopted here for the nonlinear viscoelastic constitutive relations of concrete, which was first developed in [Leaderman 1943], and has been

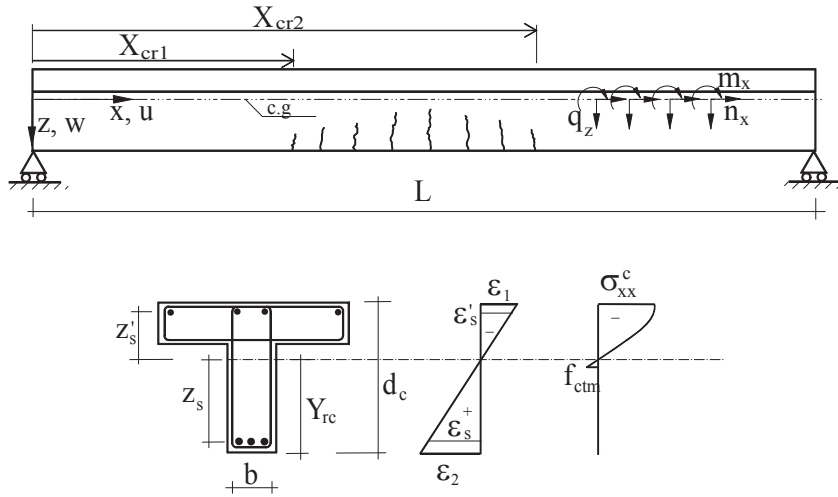


Figure 1. Geometry, loads, and sign conventions.

widely used for studying the nonlinear viscoelastic response of polymers and other materials [Pipkin and Rogers 1968; Findley et al. 1976], but with no reported application for reinforced concrete (to the best of the author's knowledge). Among other nonlinear viscoelastic models, it is chosen here as it skips over the difficulties associated with multiple integral representations (that is, evaluation of a large number of kernel functions) while still predicting the response of many materials with sufficient accuracy [Findley et al. 1976]. Following this principle, and assuming a differentiable strain history, the normal stress in concrete (σ_{xx}) takes the form

$$\sigma_{xx}(t) = \int_0^t \frac{\partial f(\varepsilon_{xx}^v(t'), t-t')}{\partial \varepsilon_{xx}^v(t')} \frac{d\varepsilon_{xx}^v(t')}{dt'} dt', \quad (1)$$

where f is a nonlinear function of strain, which represents the time-dependent stress relaxation under constant strain. Equation (1) can be rewritten in the form

$$\sigma_{xx}(t) = \int_0^t R_{xx}(\varepsilon_{xx}^v(t'), t-t') \frac{d\varepsilon_{xx}^v(t')}{dt'} dt', \quad (2)$$

with R_{xx} as the nonlinear relaxation modulus of concrete under normal strains, which introduces the effects of time-dependent cracking and material softening into the model. Under short-term loading with no creep ($t = t'$), f corresponds to the instantaneous stress as a function of the strain level, while R_{xx} actually refers to the tangent elastic modulus. Due to the lack of data on the creep behavior of concrete in shear, the formulation focuses on the concrete response under normal stresses (tension and compression), from which the response in shear is estimated. To avoid storing the entire strain history, a differential-type constitutive relation is developed, following the same concepts presented in [Taylor et al. 1970; Bažant and Wu 1974], which are further extended to the nonlinear case. To do so, the relaxation modulus needs

to be expanded into a Dirichlet series including the effect of aging of the concrete, as follows:

$$R_{xx}(\varepsilon_{xx}^v, t, t') \approx \bar{R}_{xx}(\varepsilon_{xx}^v, t, t') = \sum_{\mu=1}^N E_{\mu}(\varepsilon_{xx}^v, t') e^{-(t-t')/T_{\mu}} + E_{N+1}(\varepsilon_{xx}^v, t'), \quad (3)$$

where \bar{R}_{xx} is the approximated relaxation modulus, $E_{\mu}(\varepsilon_{xx}, t')$ is the modulus of the μ -th term in the series, N is the number of terms, and T_{μ} is the relaxation time of the μ -th term. Note that the moduli depend on the level of strain and the age of the concrete.

Following the Dirichlet series expansion, the total stress becomes the sum of the stresses of each term in the series as follows:

$$\sigma_{xx}(t) = \sum_{\mu=1}^N \sigma_{\mu}(t) + E_{N+1}(\varepsilon_{xx}^v, t) \varepsilon_{xx}^v(t). \quad (4)$$

Substitution of (3) into (2) for each term leads to

$$\sigma_{\mu}(t) = \int_0^t E_{\mu}(\varepsilon_{xx}^v, t') e^{-(t-t')/T_{\mu}} \frac{d\varepsilon_{xx}^v(t')}{dt'} dt'. \quad (5)$$

Differentiation of (5) with respect to t and rearranging the result leads to the differential equation

$$\frac{d\sigma_{\mu}}{dt} + \frac{\sigma_{\mu}}{T_{\mu}} = E_{\mu}(\varepsilon_{xx}^v, t) \frac{d\varepsilon_{xx}^v}{dt}. \quad (6)$$

Equation (6) actually describes the stress-strain relation in a Maxwell unit with age and strain-dependent spring modulus $E_{\mu}(\varepsilon_{xx}^v, t)$ and a dashpot constant $\eta(\varepsilon_{xx}^v, t) = E_{\mu}(\varepsilon_{xx}^v, t)T_{\mu}$, while the entire nonlinear viscoelastic response is described by a nonlinear rheological generalized Maxwell model following (4). This formulation means that with the evolution of damage, the effects of cracking and material nonlinearity are introduced via the dependent of the spring and dashpot constants at each point through the depth of the RC section on the corresponding strain level, with unchanged relaxation times. Mathematically, it means that the concepts used for the development of the incremental algorithms in [Bažant and Wu 1974; Sorvari and Hämäläinen 2010] and other studies for linear cases can basically be applied here with special consideration of the strain and age dependency of the constants.

However, it was shown in many studies [Bažant and Prasanna 1989] that the calculation of the time-dependent (due to aging) spring constants is associated with numerical difficulties that may lead to results that violate basic thermodynamic laws (negative spring constants). For this, Bažant and Prasanna [1989] have developed a solidification theory for creep to overcome these difficulties. Nevertheless, it was shown in [Carol and Bažant 1993] that the solidification model is equivalent to the well-known rheologic Maxwell or Kelvin models but with spring constants that increase proportionally to the same function $v(t)$, which actually describes the increase in the macroscopic elastic modulus over time, and guarantees continuously increasing positive values for the spring constants. In the linear (strain-independent) case considered in [Carol and Bažant 1993], the age-dependent spring moduli are defined by $E_{\mu}(t) = v(t)E_{\mu}$. However, in the nonlinear case considered here, the aging function represents the time variation of the macroscopic tangent modulus; apart from its normal variation with time due to aging, it depends on the level of stress or its corresponding instantaneous strain. The spring moduli in this case are given by $E_{\mu}(\varepsilon_{xx}^v, t) = v(\varepsilon_{xx}^{\text{ins}}, t)E_{\mu}(\varepsilon_{xx}^v)$ for any given pair of instantaneous and viscoelastic strains which

varies with time due to creep and stress redistribution. The derivation of the aging function is given in Section 3.3. For completeness of the formulation and for clarity, the basic steps undertaken in the derivation of the incremental procedure, which follow [Bažant and Wu 1974; Sorvari and Hämäläinen 2010], are presented here.

Assuming that the time of concern is subdivided into n_t discrete times with $\Delta t = t_r - t_{r-1}$ ($r = 1, 2, n_t$), the exact solution of (6) with initial condition $\sigma_\mu(t) = \sigma_\mu(t_{r-1})$ at $t = t_{r-1}$ is given by

$$\sigma_\mu(t_r) = e^{-\Delta t/T_\mu} \sigma_\mu(t_{r-1}) + \int_{t_{r-1}}^{t_r} e^{-(t_r-t')/T_\mu} v(\varepsilon_{xx}^{\text{ins}}(t'), t') E_\mu(\varepsilon_{xx}^v(t')) \frac{d\varepsilon_{xx}^v(t')}{dt'} dt'. \quad (7)$$

In order to evaluate the integral in (7), the strain rate, the aging function, and the spring modulus are assumed constant within the time interval provided that sufficiently small time steps that guarantee small changes of these parameters within the time interval are used. Equation (7) then becomes

$$\sigma_\mu(t_r) = e^{-\Delta t/T_\mu} \sigma_\mu(t_{r-1}) + E_\mu(\varepsilon_{xx}^v(t_r)) v(\varepsilon_{xx}^{\text{ins}}(t_r), t_r) \frac{\Delta \varepsilon_{xx}^v}{\Delta t} T_\mu [1 - e^{-\Delta t/T_\mu}]. \quad (8)$$

Using (4) and (8), the following incremental constitutive relation can be obtained for the response at $t = t_r$:

$$\Delta \varepsilon_{xx} = \frac{\Delta \sigma_{xx}}{E_c''(\varepsilon_{xx}^v(t_r))} + \Delta \varepsilon_c''(\varepsilon_{xx}^v(t_r)), \quad (9)$$

where E_c'' is the pseudonormal modulus, and $\Delta \varepsilon_c''$ is the incremental prescribed normal strain that includes both the effects of creep and shrinkage. These are given as follows:

$$E_c''(\varepsilon_{xx}^v(t_r)) = v(\varepsilon_{xx}^{\text{ins}}(t_r), t_r) \left[\sum_{\mu=1}^N [1 - e^{-\Delta t/T_\mu}] \frac{T_\mu}{\Delta t} E_\mu(\varepsilon_{xx}^v(t_r)) + E_{N+1}(\varepsilon_{xx}^v(t_r)) \right], \quad (10)$$

$$\Delta \varepsilon_c''(\varepsilon_{xx}^v(t_r)) = \frac{1}{E_c''(\varepsilon_{xx}^v(t_r))} \sum_{\mu=1}^N [1 - e^{-\Delta t/T_\mu}] \sigma_\mu(t_{r-1}) + \Delta \varepsilon_{\text{sh}}. \quad (11)$$

For brevity, the incremental constitutive relation in shear is not given here, but it follows the same procedure outlined above with G_c'' as the pseudoshear modulus and γ_c'' as the prescribed creep engineering shear strain. The next section describes the constitutive relations at the section level of the RC beam, while the determination of the spring constants and other parameters appears in Section 3.

2.2. Constitutive relations at the section level. Following Timoshenko beam theory, the incremental kinematic relations are given as follows assuming small displacements:

$$\Delta \varepsilon_{xx}(x, z) = \frac{d}{dx}(\Delta u) - z \frac{d}{dx}(\Delta \phi), \quad (12)$$

$$\Delta \gamma_{xz}(x) = \frac{d}{dx}(\Delta w) - \Delta \phi, \quad (13)$$

where γ_{xz} is the engineering shear strain and w , u , and ϕ are the vertical displacement, the in-plane displacement at the reference line, and the rotation of the cross section, respectively.

The constitutive relations at the cross-section level are determined using the classical definition of the stress resultants and (9) as follows:

$$\Delta N_{xx} = \int_{Y_c-d_c}^{Y_c} b E_c'' [\Delta \varepsilon_{xx} - \Delta \varepsilon_c''] dz + E_s \Delta \varepsilon_s A_s + E_s' \Delta \varepsilon_s' A_s', \quad (14)$$

$$\Delta M_{xx} = \int_{Y_c-d_c}^{Y_c} b E_c'' [\Delta \varepsilon_{xx} - \Delta \varepsilon_c''] z dz + E_s \Delta \varepsilon_s A_s z_s + E_s' \Delta \varepsilon_s' A_s' z_s', \quad (15)$$

$$\Delta V_{xx} = \kappa \int_{Y_c-d_c}^{Y_c} b G_c'' [\Delta \gamma_{xz} - \Delta \gamma_c''] dz, \quad (16)$$

where b , Y_c , and d_c are the width, centroid, and depth of the RC beam, respectively (see Figure 1); E_s , ε_s , and A_s are the tangent modulus of elasticity, strain, and area of the tensioned reinforcement, respectively; E_s' , ε_s' , and A_s' are the tangent modulus of elasticity, strain, and area of the compressed reinforcement; z_s and z_s' are the distances of the steel reinforcement from the centroid of the uncracked beam (see Figure 1); and κ is the shear correction factor. E_c'' , G_c'' , $\Delta \varepsilon_c''$, and $\Delta \gamma_c''$ actually depend on the strain level at each material point based on (10) and (11); hence, they vary through the depth and length of the RC beam and introduce the effects of cracking and material nonlinearity at the section level. For brevity, the notation of the dependency of these parameters on the strain level is omitted. Also E_s and E_s' depend on the strain level and introduce the effect of yielding of the steel reinforcement into the model.

Substitution of the kinematic relations, (12) and (13), into (14)–(16) yields

$$\begin{bmatrix} \Delta N_{xx} \\ \Delta M_{xx} \\ \Delta V_{xx} \end{bmatrix} = \begin{bmatrix} A_{11} & B_{11} & 0 \\ B_{11} & D_{11} & 0 \\ 0 & 0 & \kappa A_{55} \end{bmatrix} \begin{bmatrix} \frac{d}{dx}(\Delta u) \\ -\frac{d}{dx}(\Delta \phi) \\ \frac{d}{dx}(\Delta w) - \Delta \phi \end{bmatrix} - \begin{bmatrix} \Delta \bar{N} \\ \Delta \bar{M} \\ \Delta \bar{V} \end{bmatrix}, \quad (17)$$

where A_{11} , B_{11} , D_{11} , and A_{55} are the extensional, extensional-bending, flexural, and shear viscoelastic rigidities of the RC beam, and \bar{N} , \bar{V} , and \bar{M} are incremental effective forces and bending moment due to creep and shrinkage. The viscoelastic rigidities take the form

$$\begin{aligned} A_{11} &= \int_{Y_c-d_c}^{Y_c} b E_c'' dz + E_s A_s + E_s' A_s', & B_{11} &= \int_{Y_c-d_c}^{Y_c} b E_c'' z dz + E_s A_s z_s + E_s' A_s' z_s', \\ D_{11} &= \int_{Y_c-d_c}^{Y_c} b E_c'' z^2 dz + E_s A_s z_s^2 + E_s' A_s' (z_s')^2, & A_{55} &= \int_{Y_c-d_c}^{Y_c} b G_c'' dz. \end{aligned} \quad (18)$$

The incremental effective forces due to creep and shrinkage are obtained by substitution of (11) into (14)–(16) and by assuming a constant shrinkage strain profile over the depth of the RC section as follows:

$$\Delta \bar{N} = \int_{Y_c-d_c}^{Y_c} b \sum_{\mu=1}^N [1 - e^{-\Delta t/T_\mu}] \sigma_\mu^c(t_{r-1}) dz + [A_{11} - E_s A_s - E_s' A_s'] \Delta \varepsilon_{sh}, \quad (19)$$

$$\Delta \bar{M} = \int_{Y_c-d_c}^{Y_c} b \sum_{\mu=1}^N [1 - e^{-\Delta t/T_\mu}] \sigma_\mu^c(t_{r-1}) z dz + [B_{11} - E_s A_s z_s - E_s' A_s' z_s'] \Delta \varepsilon_{sh}, \quad (20)$$

$$\Delta \bar{V} = \kappa \int_{Y_c - d_c}^{Y_c} b \sum_{\mu=1}^N [1 - e^{-\Delta t/T_\mu}] \tau_\mu^c(t_{r-1}) dz. \quad (21)$$

2.3. Incremental governing equations. The incremental equilibrium equations of the RC beam, which can be found in any textbook of structural mechanics, take the form

$$\frac{d}{dx}(\Delta N_{xx}) = -\Delta n_x, \quad \frac{d}{dx}(\Delta V_{xx}) = -\Delta q_z, \quad \frac{d}{dx}(\Delta M_{xx}) - \Delta V_{xx} = \Delta m_x, \quad (22)$$

where N_{xx} , V_{xx} , and M_{xx} are the axial force, shear force, and bending moment, respectively, and q_z , n_x , and m_x are external distributed loads and bending moments, respectively. Substitution of the constitutive relations, (17), into the incremental equilibrium equations, (22), leads to the following first-order incremental governing differential equations in terms of the unknown deformations and internal forces:

$$\frac{d}{dx}(\Delta w) = (A_{55} \Delta \phi + \Delta \bar{V} + \Delta V_{xx})/A_{55}, \quad (23)$$

$$\frac{d}{dx}(\Delta \phi) = [B_{11}(\Delta N_{xx} + \Delta \bar{N}) - A_{11}(\Delta M_{xx} + \Delta \bar{M})]/(A_{11} D_{11} - B_{11}^2), \quad (24)$$

$$\frac{d}{dx}(\Delta M_{xx}) = \Delta m_x + \Delta V_{xx}, \quad \frac{d}{dx}(\Delta V_{xx}) = -\Delta q_z, \quad \frac{d}{dx}(\Delta N_{xx}) = -\Delta n_x, \quad (25)$$

$$\frac{d}{dx}(\Delta u) = [D_{11}(\Delta N_{xx} + \Delta \bar{N}) - B_{11}(\Delta M_{xx} + \Delta \bar{M})]/(A_{11} D_{11} - B_{11}^2). \quad (26)$$

2.4. Solution procedure. At each time step, (23)–(26) present a spatial set of nonlinear differential equations due to the dependency of the rigidities on the unknown deformations via (18). In general, these rigidities may vary along the uncracked and cracked regions due to the material nonlinearity. Here, a piecewise uniform distribution of the rigidities is assumed along the cracked (smeared cracking) and uncracked regions. Thus, the rigidities along the cracked region are determined based on analysis of the critical cross section, while the rigidities at the uncracked region are assumed strain-independent. This defines two types of parameters that need to be determined at each time step, namely: the rigidities at the critical section, and the start and end locations of the cracked region (X_{cr1} and X_{cr2} ; see Figure 1). An iterative procedure is used for the determination of these parameters at each time step, while due to the piecewise variation of the rigidities and the continuous variation along the beam of the incremental effective forces due to creep and shrinkage, a numerical technique that is based on the multiple shooting method [Stoer and Bulirsch 2002] is adopted for the solution of the equations at each iteration. The iterative procedure basically follows [Rabinovitch and Frostig 2001; Hamed and Rabinovitch 2008] but it is slightly modified here to account for the viscoelastic response, as follows:

Step 1. Initial guess. At the first iteration of the first increment of instantaneous loading, the beam is assumed uncracked. However, for the progressive time steps (load increment), the solution from the previous time step is used as the initial guess for the current step.

Step 2. Analysis of the structure. Using the rigidities calculated in the initial guess or in the previous iteration (Step 3.3), as well as the calculated locations of the start and end points of the cracked region, the incremental governing equations become linear ones with variable coefficients in space, which are solved numerically.

Step 3. Analysis of the critical section (at the location of maximum moment). Based on the solution obtained in Step 2, the equivalent rigidities of the critical section are determined as follows:

3.1 A linear distribution of the incremental total strain is assumed:

$$\Delta\varepsilon_{xx} = \frac{\Delta\varepsilon_1 + \Delta\varepsilon_2}{2} - \frac{\Delta\varepsilon_1 - \Delta\varepsilon_2}{d_c}z, \quad (27)$$

where $\Delta\varepsilon_1$ and $\Delta\varepsilon_2$ are the incremental strains at the upper and lower faces of the RC beam, as shown in Figure 1.

3.2 Based on the incremental internal forces obtained in Step 2, two nonlinear algebraic equations are stated in terms of the two unknowns $\Delta\varepsilon_1$ and $\Delta\varepsilon_2$, which are based on equilibrium of forces and moments at the current time step, as follows:

$$\Delta N_{xx} = \int_{Y_c-d_c}^{Y_c} b \Delta\sigma_{xx} dz + E_s \Delta\varepsilon_s A_s + E'_s \Delta\varepsilon'_s A'_s, \quad (28)$$

$$\Delta M_{xx} = \int_{Y_c-d_c}^{Y_c} b \Delta\sigma_{xx} z dz + E_s \Delta\varepsilon_s A_s z_s + E'_s \Delta\varepsilon'_s A'_s z'_s, \quad (29)$$

where $\Delta\sigma_{xx}$ is defined via (9). As creep in RC beams tends to shift the neutral axis downwards [Gilbert 1988], the tensile capacity of already-cracked material points under instantaneous loading is set to zero in solving (28) and (29) with time.

3.3 Once the normal strain distribution is determined in Step 3.2, as well as the corresponding normal and shear stresses, the spring moduli of each point through the depth of the RC beam are determined. Consequently, the viscoelastic rigidities and the incremental effective forces due to creep and shrinkage are determined through (18) and (19)–(21), respectively.

Step 4. Convergence criterion. If the norm of the relative difference between the magnitudes of the viscoelastic rigidities, as well as X_{cr1} and X_{cr2} , in two successive iterations is sufficiently small, the iterative procedure stops. Otherwise, the procedure returns to Step 2 with the updated rigidities of Step 3.3.

3. Material properties and model parameters

The incremental mathematical model developed in Section 2 is valid for any desired creep model and material properties provided that the strain-dependent relaxation modulus and the corresponding spring moduli of the Maxwell model are known. Here, the specific viscoelastic models that are adopted in the numerical study, and which can be used for the analysis of most RC structures, are discussed, along with the determination of the model parameters (that is, relaxation modulus and spring and dashpot constants).

3.1. Nonlinear relaxation modulus of concrete. Before the characterization of the nonlinear relaxation modulus, the instantaneous stress-strain law, from which the viscoelastic constitutive relations are derived, is presented. The material properties and material models are taken from [CEB-FIP 1990; 1999] with

the following instantaneous stress-strain relation that is also shown in Figure 2:

$$\sigma_{xx} = \begin{cases} \frac{E_0 \varepsilon_{xx}^{ins} + f_{cm} \frac{(\varepsilon_{xx}^{ins})^2}{\varepsilon_c^2}}{1 - \left(\frac{E_0 \varepsilon_c}{f_{cm}} + 2\right) \frac{\varepsilon_{xx}^{ins}}{\varepsilon_c}} & \text{for } \varepsilon_{lim}^c \leq \varepsilon_{xx}^{ins} \leq \varepsilon_{cr}, \\ f_{ctm} + E_d (\varepsilon_{xx}^{ins} - \varepsilon_{cr}) & \text{for } \varepsilon_{cr} < \varepsilon_{xx}^{ins} \leq \varepsilon_{lim}^t, \\ 0 & \text{for } \varepsilon_{lim}^t < \varepsilon_{xx}^{ins}, \end{cases} \quad (30)$$

where f_{cm} is the mean compressive strength that equals $f_{ck} + 8$ (in MPa) with f_{ck} being the characteristic strength, E_0 is the modulus of elasticity, ε_c is the strain at peak compressive stress, ε_{cr} is the cracking strain (determined based on the mean tensile strength as f_{ctm}/E_0), and ε_{lim}^c is the strain that corresponds to a stress of $0.5 f_{cm}$ at the descending part of the diagram; further, $E_d = -0.483 E_0 / (0.393 + f_{ctm})$ describes the tension-softening effect [Bažant and Oh 1984], and $\varepsilon_{lim}^t = \varepsilon_{cr} - f_{ctm}/E_d$.

The stress-strain curve of the steel is based on a linear elastic-perfectly plastic behavior with ε_y as the yielding strain as follows:

$$\sigma_s = \begin{cases} E_s \varepsilon_s & \text{for } -\varepsilon_y \leq \varepsilon_s \leq \varepsilon_y, \\ E_s \varepsilon_y & \text{otherwise.} \end{cases} \quad (31)$$

The failure criteria in tension and compression are based on limit strains in order to account for the creep rupture effects. Under instantaneous loading, cracking occurs once ε_{xx}^{ins} becomes greater than ε_{cr} . For simplicity, the strain-softening effect is ignored and the stresses are assumed to drop immediately to zero upon cracking. Many studies show that the effects of tension-softening and tension-stiffening are mostly dominant in lightly reinforced structures, which is not the case in most RC beams [Gilbert 2007]. Under sustained loading, on the other hand, it is assumed that creep rupture in tension occurs when the viscoelastic strain (creep curve) intersects the descending part of the stress-strain curve [Zhou 1994], allowing ε_{xx}^v to exceed ε_{cr} without immediate failure as observed in some experimental studies and shown in Figure 2. In other words, it is assumed that the instantaneous stress-strain curve serves

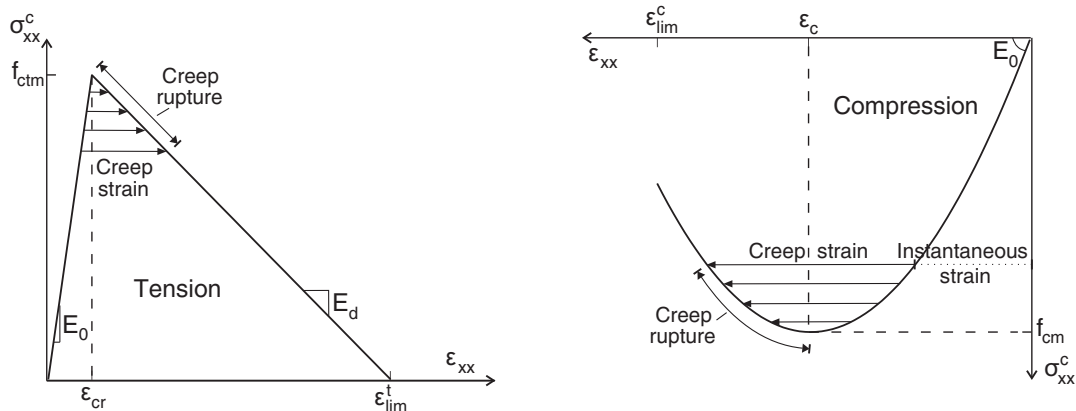


Figure 2. Stress-strain curves of concrete under tension and compression.

as an envelope failure criterion. Following this procedure, the failure strain envelope in tension ε_f^t is given by

$$\varepsilon_f^t = \frac{\sigma_{xx}^c - f_{ctm}}{E_d} + \varepsilon_{cr}. \quad (32)$$

Thus, the relaxation modulus of any point through the depth of the RC beam, for which its viscoelastic strain exceeds its corresponding failure strain, is set to zero to simulate the creep rupture effect. Note that due to aging, the failure envelope changes with time.

As the paper focuses on the nonlinear creep response rather than the behavior under short-term loading, which is well known, failure in compression under instantaneous loading is not accounted for. Thus, it is assumed that the level of instantaneous compressive strains is smaller than ε_c (in absolute value). Nevertheless, in order to account for the creep rupture failure in compression, a limit strain failure criterion should be used. In general, the creep rupture failure envelope in compression is a descending curve from the peak static strength to a horizontal line at about $(0.7-0.8)f_{cm}$ [Carol and Murcia 1989; Omar et al. 2009]. Here, it is assumed that this descending curve is similar to the descending (strain softening) part of the stress-strain curve given in (30), indicating that also under compression, creep rupture occurs once the viscoelastic strain intersects the stress-strain diagram as shown in Figure 2 [Fernández Ruiz et al. 2007]. Such similarity between the modeling of damage due to creep and material nonlinearity under short term loading is owned to the similarities in their sources, which correspond to interfacial bond microcracks between the aggregates and the mortar, and microcracking of the mortar material itself [Bažant and Asghari 1977; Li and Qian 1989]. Using the strain-softening part of (30) in compression, the failure strain envelope in compression ε_f^c takes the form

$$\varepsilon_f^c = \frac{-E_0 - \frac{E_0\sigma_{xx}}{f_{cm}} - \frac{2\sigma_{xx}}{\varepsilon_c} - \left[\left(E_0 + \frac{E_0\sigma_{xx}}{f_{cm}} + \frac{2\sigma_{xx}}{\varepsilon_c} \right)^2 + 4 \frac{f_{cm}\sigma_{xx}}{\varepsilon_c^2} \right]^{1/2}}{2f_{cm}/\varepsilon_c^2}. \quad (33)$$

Based on these assumptions, the nonlinear relaxation functions should be defined for the uncracked material points with $\varepsilon_c \leq \varepsilon_{xx}^{\text{ins}} \leq \varepsilon_{cr}$ while ε_{xx}^v can be greater than ε_{cr} or ε_c (in absolute value) as shown in Figure 2.

The determination of the relaxation modulus is based on the compliance modulus because of the limited experimental data available for its calibration. Nevertheless, the well-known convolution integral relation between the relaxation and compliance moduli is not valid for nonlinear materials [Findley et al. 1976]. This introduces some difficulties in the determination of the nonlinear relaxation modulus, also because, as shown in [Oza et al. 2003], a separable nonlinear compliance (between time and stress) normally leads to a nonseparable form of a relaxation modulus. Oza et al. [2003] provided closed-form expressions of the nonlinear relaxation modulus for some specific compliance moduli of ligaments and metals based on a single integral nonlinear superposition method. Other numerical approaches for obtaining the nonlinear relaxation modulus from the compliance modulus at each time step were developed in [Brueller and Steiner 1993; Touati and Cederbaum 1997]. Here, the relaxation modulus is estimated based on a trial and error method seeking a closed-form expression. This is based on the physical meaning of the kernels in (1) and the corresponding creep equation given below (see [Findley

et al. 1976]):

$$\varepsilon_{xx}^v(t) = \int_0^t \frac{\partial g(\sigma_{xx}(t'), t-t')}{\partial \sigma_{xx}(t')} \frac{d\sigma_{xx}(t')}{dt'} dt', \quad (34)$$

where g is a nonlinear function of stress, which represents the time-dependent viscoelastic strain under constant stress, and $\partial g/\partial \sigma_{xx}$ is the nonlinear compliance modulus. The problem actually reduces to finding a general stress history $\sigma_{xx}(t) = \sigma_h(t)$, such that when inserted into (34), then the obtained viscoelastic strain $\varepsilon_{xx}^v(t)$ becomes constant with time and equals to a desired value (ε_{xx}^0). In other words, since creep and relaxation are two aspects of the same viscoelastic material behavior, then the time-dependent stress (function f in (1)) that will be obtained in a relaxation test under a certain value of strain is exactly the same one that needs to be used in a stress-varying creep test ($\sigma_{xx}(t) = \sigma_h(t)$ in (34)) to obtain the same constant strain value.

Using the ascending part (in absolute value) of the short-term stress-strain relation of the concrete, (30), the function g in (34) takes the following separable form for $f_{cm} \leq \sigma_{xx} \leq f_{ctm}$:

$$g = \frac{-E_0 - \frac{E_0 \sigma_{xx}}{f_{cm}} - \frac{2\sigma_{xx}}{\varepsilon_c} + \left[\left(E_0 + \frac{E_0 \sigma_{xx}}{f_{cm}} + \frac{2\sigma_{xx}}{\varepsilon_c} \right)^2 + 4 \frac{f_{cm} \sigma_{xx}}{\varepsilon_c^2} \right]^{1/2}}{2f_{cm}/\varepsilon_c^2} (1 + \varphi(t)), \quad (35)$$

where $\varphi(t)$ is the creep coefficient that is evaluated based on [CEB-FIP 1990]. Note that in this simplified formulation, the nonlinearity between stresses and creep strains is modeled through the constitutive law only [Bockhold and Petryna 2008] and not through a stress-dependent creep coefficient [CEB-FIP 1990; Fernández Ruiz et al. 2007].

Following the procedure outlined above, different potential stress histories ($\sigma_{xx}(t) = \sigma_h(t)$) need to be introduced into (34). The one that leads to constant strain values with time at different levels of initial strain is the one that corresponds to the function f in (1), which will be used for the derivation of the relaxation modulus. The basis for choosing such stress histories is that they should actually be decreasing functions with time and have to fulfill the instantaneous stress-strain relation at $t = 0$. The following general form is proposed with ε_{xx}^0 being the desired constant strain value:

$$\sigma_h(t) = \frac{\frac{1}{(1+\varphi(t))^\alpha} \left(E_0 \varepsilon_{xx}^0 + \frac{f_{cm}}{(1+\varphi(t))^\zeta} \frac{(\varepsilon_{xx}^0)^2}{\varepsilon_c^2} \right)}{1 - \left(\frac{E_0 \varepsilon_c}{f_{cm}} + 2 \right) \frac{\varepsilon_{xx}^0}{\varepsilon_c}}. \quad (36)$$

Figure 3 shows the normalized time variation of the strain at different levels obtained from different stress histories with different values of α and ζ (see (36)). For this illustration, f_{cm} is taken as 38 MPa, $\varepsilon_c = -0.224\%$, and $E_0 = 33.5$ GPa. The creep coefficient is assumed to follow [CEB-FIP 1990] as $\varphi(t) = \varphi_u t^{0.3}/(t + \beta_H)^{0.3}$ with $\varphi_u = 2.11$ and $\beta_H = 459$. The integration of (34) is achieved using an incremental time-stepping numerical integration, assuming a constant compliance function (averaged over two consecutive times) during each time interval following a nonlinear superposition approach [Oza et al. 2003; Hamed et al. 2011]. It can be seen that at the low level of initial strain ($0.05\varepsilon_c$), all stress histories reveal a very small change of the normalized strain with time (a deviation of less than 2%). However, under higher levels of initial strains where material nonlinearity becomes significant ($0.25\varepsilon_c$ and $0.45\varepsilon_c$, that correspond to stresses of $0.43f_{cm}$ and $0.7f_{cm}$, respectively), only the stress history with

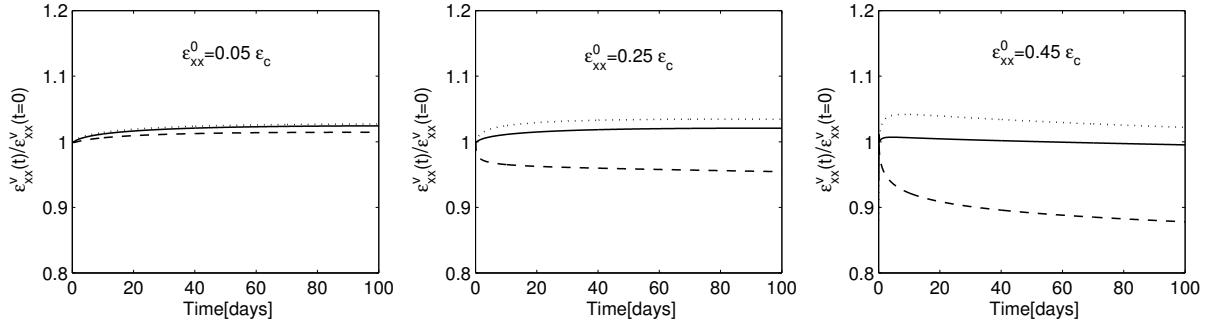


Figure 3. Variation of strain in time under different decreasing stress histories at different levels of initial strain (the solid line indicates $\alpha = 1, \zeta = 1$; the dashed $\alpha = 1, \zeta = 0$; and the dotted $\alpha = 1, \zeta = 2$).

$\alpha = \zeta = 1$ still yields a very small change, while stress histories achieved with other values of α and ζ reveal significantly varying strains with time. Hence, the function f is assumed to take the form of (36) with $\alpha = \zeta = 1$ and replacing ε_{xx}^0 with ε_{xx}^v . It has to be mentioned that the exercise outlined in Figure 3 has been implemented at various material properties to verify the validity of the chosen function f . No doubt a more accurate method to evaluate the function f would be one based on minimization of the error at each time step [Brueller and Steiner 1993; Touati and Cederbaum 1997], but the method outlined above is chosen as it provides a closed-form solution with an acceptable accuracy.

Once the function f is defined, the nonlinear strain-dependent relaxation modulus can be obtained by differentiating f with respect to ε_{xx}^v (see (1) and (2)) to yield a closed nonseparable form of the nonlinear relaxation modulus of concrete as follows:

$$R_{xx} = \frac{E_0}{\bar{a}(1 + \varphi(t))} + \frac{E_0 \varepsilon_{xx}^v}{\bar{a}(1 + \varphi(t))} \left[\frac{2f_{cm}}{E_0 \varepsilon_c^2} + \frac{E_0}{\bar{a} f_{cm}} + \frac{2}{\bar{a} \varepsilon_c} \right] + \frac{E_0 (\varepsilon_{xx}^v)^2}{[\bar{a}(1 + \varphi(t))]^2} \left[\frac{1}{\varepsilon_c} + \frac{2f_{cm}}{E_0 \varepsilon_c^3} \right], \quad (37)$$

where $\bar{a} = 1 - E_0 \varepsilon_{xx}^v / f_{cm} - 2\varepsilon_{xx}^v / \varepsilon_c$. For relatively small strains (that is, $0.15\varepsilon_c \leq \varepsilon_{xx}^v \leq \varepsilon_{cr}$), the second and third terms are relatively small and $\bar{a} \approx 1$; thus, (37) yields the classical approximated form of the relaxation modulus of a linear viscoelastic material as $\approx 1/J_{xx}$ (with J_{xx} as the compliance function). Also note that for $\varphi(t) = 0$, (37) yields the strain-dependent tangent modulus of concrete.

The effect of aging on the nonlinear relaxation modulus is introduced through the development of f_{cm} , E_0 , and ε_c with time as follows [CEB-FIP 1990; 1999]:

$$f_{cm}(t) = (f_{ck} + 8) \exp \left\{ 0.25 \left[1 - \left(\frac{28}{t} \right)^{1/2} \right] \right\}, \quad (38)$$

$$E_0(t) = \sqrt{\frac{f_{cm}(t)}{f_{cm}(28)}} E_0(28), \quad (39)$$

$$\varepsilon_c(t) = -0.0017 - 0.001(f_{cm}(t))/70, \quad (40)$$

where t refers to the age of concrete in days, and f_{ck} and f_{cm} are in MPa. The development of the tensile

strength f_{ctm} with time is assumed to follow that of the compressive strength, which is given by

$$f_{ctm} = \frac{f_{cm}(t)}{f_{cm}(28)} 1.4 \left(\frac{f_{ck}}{10} \right)^{2/3}. \quad (41)$$

3.2. Springs and dashpot constants in Maxwell model. Given the strain and age-dependent relaxation modulus appears in (37) and the relation $E_\mu(\varepsilon_{xx}^v, t) = v(\varepsilon_{xx}^{ins}, t) E_\mu(\varepsilon_{xx}^v)$ described earlier, the strain-dependent spring and dashpot constants of the Maxwell model can be obtained by a least squares or other curve-fitting method following (3). Thus, for any given strain level, the relaxation function given in (37) is expanded into a Dirichlet series, (3), and the Maxwell constants are determined. For this, the relaxation times and the number of units are chosen in advance considering the time of interest [Bažant and Wu 1974], and the moduli of the springs become the only unknowns in the generalized Maxwell chain. A least squares method that was proposed in [Bažant and Wu 1974] is used here for the determination of the spring moduli, which is based on minimization the following expression ($d\Phi/dE_\mu$):

$$\begin{aligned} \Phi = & \sum_i^{N_t} [\bar{R}_{xx}(\varepsilon_{xx}^v, t_i) - R_{xx}(\varepsilon_{xx}^v, t_i)]^2 + \omega_1 \sum_{\mu=1}^{N-1} [E_{\mu+1}(\varepsilon_{xx}^v) - E_\mu(\varepsilon_{xx}^v)]^2 \\ & + \omega_2 \sum_{\mu=1}^{N-2} [E_{\mu+2}(\varepsilon_{xx}^v) - 2E_{\mu+1}(\varepsilon_{xx}^v) + E_\mu(\varepsilon_{xx}^v)]^2 \\ & + \omega_3 \sum_{\mu=1}^{N-3} [E_{\mu+3}(\varepsilon_{xx}^v) - 3E_{\mu+2}(\varepsilon_{xx}^v) + 3E_{\mu+1}(\varepsilon_{xx}^v) - E_\mu(\varepsilon_{xx}^v)]^2, \quad (42) \end{aligned}$$

where N_t is the number of selected times for which minimization of the error is conducted, and ω_1 , ω_2 , and ω_3 are weight functions that are determined to achieve best fitting.

Nevertheless, in order to avoid calculation of the spring moduli via minimization of (42) at each strain level, the calculation is made here at a number of selected strain levels (N_ε) along with the use of an interpolation function for each spring modulus to obtain a continuous variation. The following interpolation function is used for the μ -th spring modulus:

$$E_\mu(\varepsilon_{xx}^v) \approx \bar{E}_\mu(\varepsilon_{xx}^v) = c_{1\mu} + c_{2\mu} \varepsilon_{xx}^v + c_{3\mu} (\varepsilon_{xx}^v)^2 + c_{4\mu} (\varepsilon_{xx}^v)^3 + c_{5\mu} (\varepsilon_{xx}^v)^4. \quad (43)$$

Note that after the minimization of (42) at N_ε strain levels, a series of N_ε values is obtained for every spring modulus, from which the interpolation function that appears in (43) is determined. Also here, the constants $c_{1\mu}$ to $c_{5\mu}$ are determined by traditional least squares or other curve-fitting methods.

However, due to the creep rupture phenomenon of concrete, the spring moduli actually follow (43) up to certain levels of strains. The final expression for the spring moduli under normal stresses takes the form

$$E_\mu^c(\varepsilon_{xx}^v) = \begin{cases} \bar{E}_\mu(\varepsilon_{xx}^v) & \text{for } \varepsilon_f^c \leq \varepsilon_{xx}^v \leq \varepsilon_f^t, \\ 0 & \text{otherwise.} \end{cases} \quad (44)$$

Thus, the spring moduli of any point through the depth of the RC beam, for which its viscoelastic strain exceeds its corresponding failure strain, is set to zero to simulate the creep rupture failure.

The spring moduli in shear are estimated from (44) assuming that Poisson's ratio ν and the shear retention factor β , which simulates the shear resistance at the cracked interfaces owing to the aggregate interlock and dowel action [Rots and de Borst 1987], are constant with time and independent upon the stress level. Thus, using the same relaxation times and number of units as in the normal direction, the spring moduli in shear take the form

$$G_{\mu}^c(\varepsilon_{xx}^v) = \begin{cases} \frac{\bar{E}_{\mu}(\varepsilon_{xx}^v)}{2(1+\nu)} & \text{for } \varepsilon_f^c \leq \varepsilon_{xx}^v \leq \varepsilon_f^t, \\ \frac{\beta \bar{E}_{\mu}(\varepsilon_f^t)}{2(1+\nu)} & \text{for } \varepsilon_f^t < \varepsilon_{xx}^v, \\ 0 & \text{otherwise.} \end{cases} \quad (45)$$

3.3. Aging function. As mentioned earlier, the effect of aging is introduced through the function $v(\varepsilon_{xx}^{\text{ins}}, t)$, which is evaluated based on the time-variation of the tangent elastic modulus with respect to its magnitude at the time of initial loading. Setting $\varphi(t) = 0$ in (37) along with replacing the viscoelastic strain (ε_{xx}^v) by the instantaneous one ($\varepsilon_{xx}^{\text{ins}}$) as a result, and the use of (38)–(40), lead to a closed-form expression for the time-dependent tangent elastic modulus $E_t(\varepsilon_{xx}^{\text{ins}}, t) = R_{xx}$, which for brevity is not presented here. Then $v(\varepsilon_{xx}^{\text{ins}}, t)$ can be evaluated as $E_t(\varepsilon_{xx}^{\text{ins}}, t)/E_t(\varepsilon_{xx}^{\text{ins}}, t_0)$, where t_0 corresponds to the age of the concrete at the time of initial loading.

4. Numerical study

The numerical study includes two numerical examples and parametric studies that highlight and clarify the nonlinear creep response of RC beams, and exhibit the capabilities of the proposed model. A comparison of the model with test results available in the literature is also included.

4.1. First example: Beam under bending only. A simply supported RC beam, 4.0 m long and with a rectangular cross-section 200 mm wide and 400 mm high is used for the investigation. The beam includes two bars of 24 mm diameter (a reinforcement ratio of $\rho_s = 1.2\%$) located at 30 mm from the bottom ($z_s = 170$ mm) with $E_s = 200$ GPa, and is subjected to a uniformly distributed sustained load of 60 kN/m. The modulus of elasticity and mean compressive strength of the concrete are taken as $E_0 = 33.5$ GPa and $f_{\text{cm}} = 38$ MPa, while the tensile strength and peak compressive strain are $f_{\text{ctm}} = 2.91$ MPa and $\varepsilon_c = -0.22\%$ following (40) and (41). The development in time of the creep coefficient and shrinkage strain follows [CEB-FIP 1990] with ultimate values of $\varphi_u = 2.11$ and $\varepsilon_{\text{sh}}(t = \infty) = -0.042\%$. The Poisson's ratio, the shear retention factor, and the shear correction factor are taken as 0.17, 0.2, and 0.833, respectively. In order to highlight the effect of creep only, the effects of shrinkage and compressive reinforcement are not considered at this stage, but are separately investigated in the subsequent. The analysis is conducted up to 3 years from first loading where the creep coefficient reaches a magnitude of 1.9. Seven Maxwell units are used in the material model along with the use of (43) to account for the nonlinear variation of the Maxwell constants with the strain level. The relaxation times are chosen as $T_{\mu} = 0.1 \times 5^{\mu-1}$ days, for $\mu = 1, \dots, 6$, and the spring moduli take the following strain-dependent form

(in GPa) following (43):

$$\begin{bmatrix} \bar{E}_1 \\ \bar{E}_2 \\ \bar{E}_3 \\ \bar{E}_4 \\ \bar{E}_5 \\ \bar{E}_6 \\ \bar{E}_7 \end{bmatrix} = \begin{bmatrix} 5.337 & 9.962 & -0.295 & -0.757 & -0.505 \\ 1.881 & -2.916 & -0.863 & -0.289 & 0.75 \\ 3.346 & 0.026 & -0.149 & -0.32 & -0.104 \\ 4.03 & -4.88 & -0.145 & -0.388 & 0.283 \\ 3.843 & -3.736 & -0.11 & -0.446 & 0.103 \\ 3.607 & -2.491 & -0.745 & -0.282 & -0.142 \\ 11.483 & -3.509 & -0.104 & -0.308 & 0.232 \end{bmatrix} \begin{bmatrix} 1 \\ \varepsilon_{xx}^v \\ (\varepsilon_{xx}^v)^2 \\ (\varepsilon_{xx}^v)^3 \\ (\varepsilon_{xx}^v)^4 \end{bmatrix}. \quad (46)$$

Figure 4 shows the distribution of the instantaneous and long-term normal strains and stresses at midspan through the depth of the beam. The results show the nonlinear stress distribution at $t = 0$, with a maximum compressive stress of -26.8 MPa ($\approx 0.7 f_{cm}$). Due to creep, an increase in the tension force of the elastic reinforcement occurs as it tends to restrain the creep deformations. As a result, a compressive force in the concrete of equal magnitude has to develop to maintain equilibrium. Yet, because the bending moment is unchanged, the lever arm between the steel and concrete must decrease by a shifting down of the neutral axis from $z_0 = -68.9 \text{ mm}$ to $z_0 = -17.6 \text{ mm}$ as shown in Figure 4. Due to this significant shifting, the loaded area of the concrete is increased resulting in a release and redistribution of the stresses with time. Note that as this shifting occurs, the neutral axis passes through points, which were already cracked under instantaneous loading, and for which their tensile capacity is set to zero, as can be seen in the distribution of stresses 3 years after loading. These stress and strain redistributions with time, which also occur in the linear case [Gilbert 1988], are well captured and explained by the proposed model in the nonlinear range of stresses.

The time variation of the central deflection, peak curvature (defined as $\chi = d\phi/dx$), peak force in the reinforcement, and peak compressive stress in the concrete appear in Figure 5 with and without the inclusion of the aging effect in the analysis. The results are normalized with respect to the instantaneous

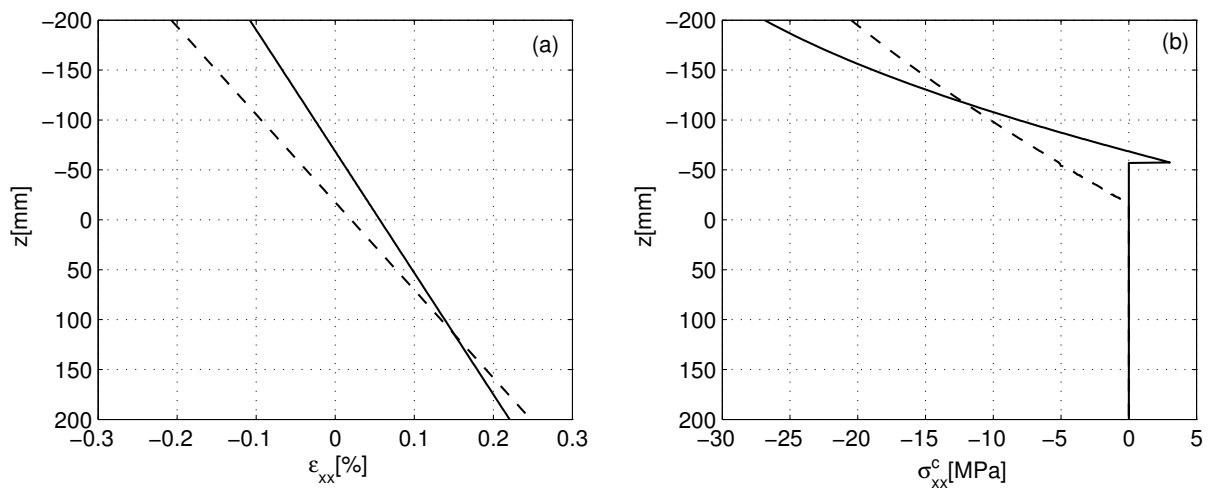


Figure 4. Normal stress and strain distributions at midspan (example 1): (a) strains and (b) stresses (the solid line is $t = 0$ and the dashed is $t = 3$ years).

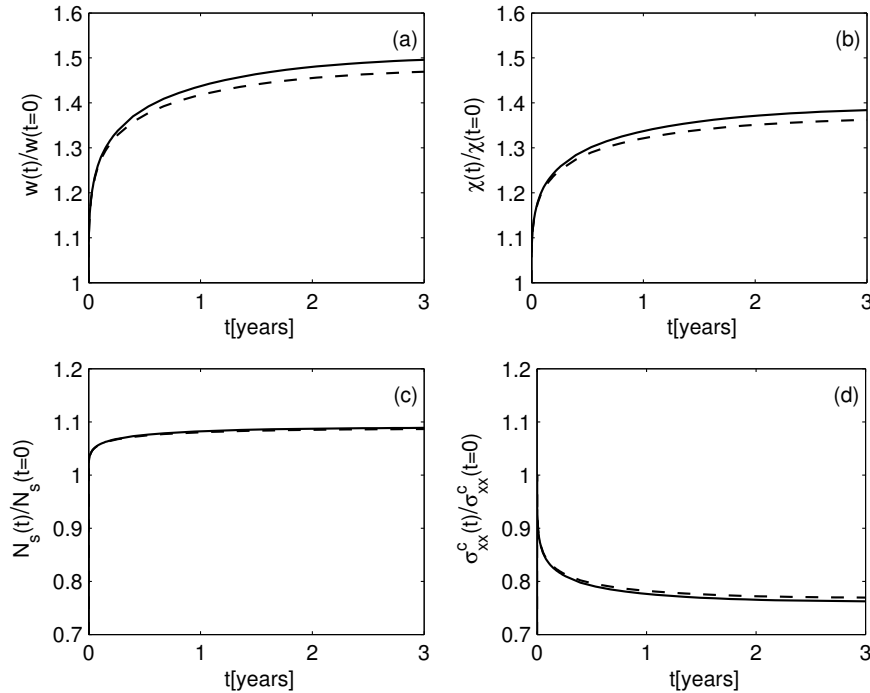


Figure 5. Normalized creep response at midspan: (a) vertical deflection, (b) curvature, (c) axial force in the reinforcement, and (d) maximum compressive stress in the concrete (the solid line indicates no aging and the dashed with aging).

response which reveal a central deflection of $w(t=0) = 13.19$ mm, a curvature of $\chi(t=0) = 0.0082$ 1/m and a peak steel force of $N_s(t=0) = 354.6$ kN. The results show that the normalized increase of the deflection is larger than that of the curvature, which in turn is much larger than the increase in the reinforcement force. Thus, creep has different effects on the structural response, which requires careful attention especially when material nonlinearity is included. Nevertheless, due to cracking and the restraint of creep by the steel reinforcement, the creep amplification of the deformations and forces is much less than 2.9, which is the case in a linear homogeneous material (other than reinforced concrete) with a creep coefficient of 1.9 after 3 years. The results also show that aging has a small effect on the deformations, along with a negligible effect on the forces and stresses. In both cases, the cracked region slightly propagates along the beam due to tensile creep rupture, and its left edge moves from $X_{cr1} = 166.7$ mm to $X_{cr1} = 150$ mm after 3 years.

To further clarify the structural response, the effects of the load level as well as the shrinkage strains are examined in Figure 6. Aging is accounted for, and all other reference parameters including the loading and material properties are kept unchanged. The instantaneous failure load of the beam is calculated as $q_z^u = 76$ kN/m, for which yielding of the steel reinforcement occurs. The results show that increasing the load level leads to a decrease in the normalized peak deflection and steel force, and consequently to a smaller release of the peak compressive stresses. A similar conclusion was also reported in [Tan and Saha 2006], yet mainly for RC beams strengthened with composite materials. No creep rupture in

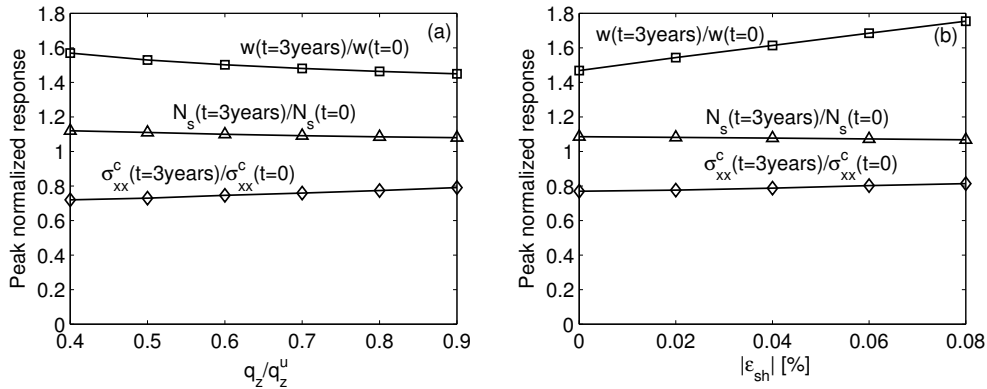


Figure 6. Effect of (a) load level and (b) shrinkage strain on the long-term response.

compression is observed in all cases examined here due to the rapid release of the peak compressive stresses a short time after loading as can be seen in Figure 5d. This is believed to be the case in most RC beams under bending only.

On the other hand, shrinkage seems to significantly increase the deflections but with much smaller effect on the axial force and stresses. The normalized long-term deflection is increased due to shrinkage from 1.47 the instantaneous deflection for $\epsilon_{sh} = 0$ to about 1.76 the instantaneous deflection for $\epsilon_{sh} = -0.08\%$; this is a significant increase of 62% in the long-term effects. Shrinkage also leads to further shifting down of the neutral axis and to a smaller increase of the reinforcement axial force and less release of the stresses as the magnitude of the shrinkage strain increases. In addition, the long-term cracking length is also affected by shrinkage, and its left edge decreases from $X_{cr1} = 150$ mm for $\epsilon_{sh} = 0$ to $X_{cr1} = 0$ for $\epsilon_{sh} \leq -0.06\%$.

The effect of the reinforcement ratio of both the compressed and tensioned steel is investigated in Figure 7. Also here, aging is accounted for, and all other reference parameters are kept unchanged; z'_s is taken as -170 mm. As indicated in many studies [Washa and Fluck 1952; Neville and Dilger 1970], the results show that the compressed steel reinforcement significantly restrains the creep effects and leads to

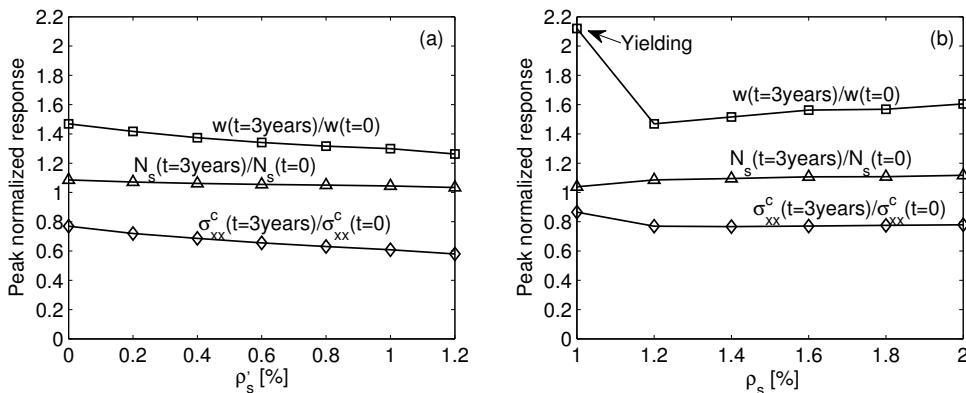


Figure 7. Effect of (a) compressed and (b) tensioned reinforcement ratios.

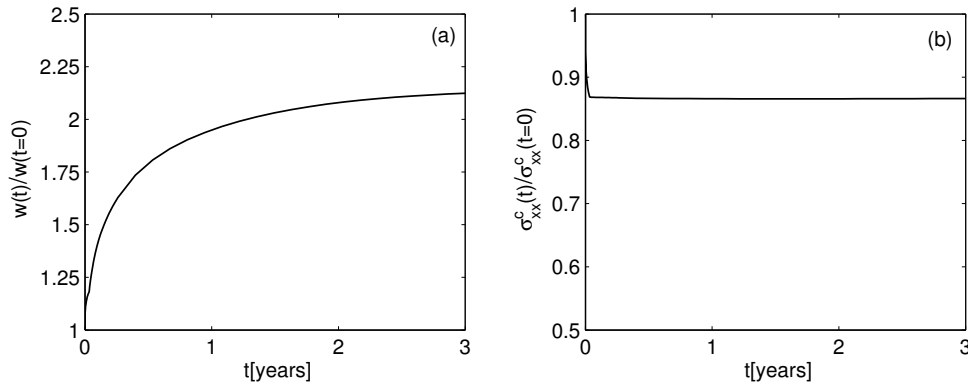


Figure 8. Normalized creep response at midspan with yielding of the reinforcement: (a) vertical deflection and (b) maximum compressive stress in the concrete.

smaller long-term deflections. The proposed model, which is able to quantitatively predict this effect for the nonlinear case, also shows that this is associated with a slight decrease of the normalized axial force, as well as a considerable release of the peak compressive stresses in the concrete.

Figure 7b shows that for $1.2\% \leq \rho_s$, increasing the tensioned reinforcement ratio leads to an increase in the normalized deflection and axial forces, and a further release of the stresses. The reason for that is the increase in the area of the cross-section under compression with the increase of the reinforcement ratio. As creep is proportional to the level of stresses, which are much larger in compression than in tension, the larger the area under compression the more creep deformations develop. The relatively high normalized deflection observed with $\rho_s = 1.0\%$ is a result of yielding with time of the tensioned reinforcement. To clarify this, the time variation of the central deflection and peak compressive stress in the concrete appear in Figure 8 for this case. After yielding of the steel reinforcement at $t = 14$ days after loading, the concrete starts to creep freely without the restraint of the reinforcement. As a result, the neutral axis remains unchanged and no further stress relaxation occurs; hence we have the relatively high peak normalized deflection, which is about 2.12.

4.2. Second example: Beam under bending and compression. The RC beam examined in Section 4.1 is investigated here under a combination of both vertical and axial compression loadings (which may simulate a beam-column or a prestressed beam). The vertical load is as earlier while the axial compression load equals 1200 kN. Aging is accounted for while no compressed reinforcement and no shrinkage effects are included in the analysis. The distributions of the instantaneous and long-term normal strains and stresses are shown in Figure 9. The results show that in this case there is a relatively small shifting of the neutral axis down as most of the beam cross-section is under compression. Consequently only a slight change in the stress distribution is observed over time. However, it can be seen that creep rupture in compression occurred at some points that were under high levels of instantaneous stresses. Although the model provides a description of the response beyond first creep rupture, unlike creep rupture in tension, the time for which first creep rupture in compression occurs can be defined as a critical time (t_{cr}) as it may initiate total failure of the structure. In this example it equals 155 days.

The time variations of the central deflection and peak force in the reinforcement are shown in Figure 10. The results are normalized with respect to the instantaneous response which reveals a central deflection of

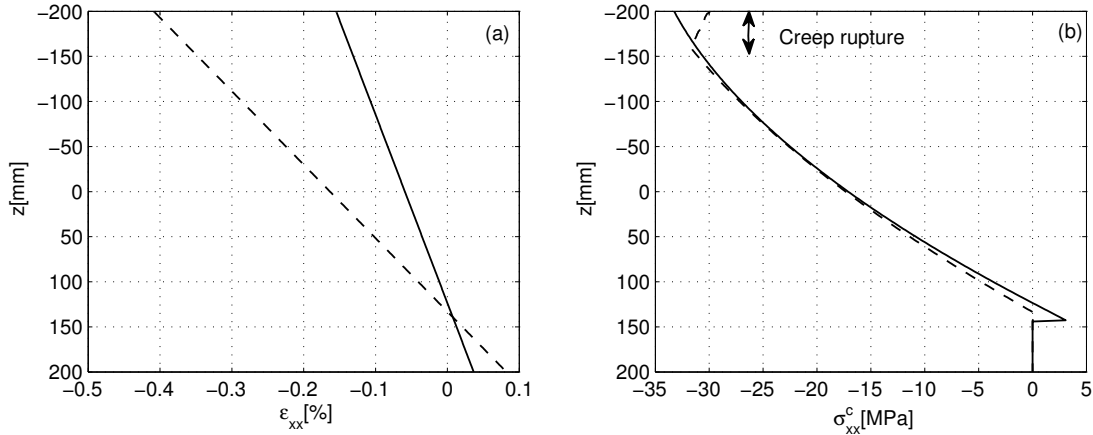


Figure 9. Normal stress and strain distributions at midspan (example 2): (a) strains and (b) stresses (the solid line is $t = 0$ and the dashed $t = 3$ years).

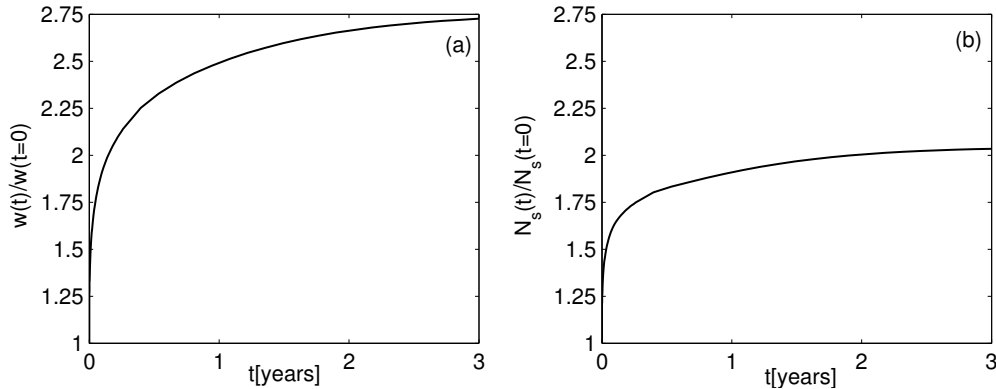


Figure 10. Normalized creep response at midspan (example 2): (a) vertical deflection and (b) axial force in the reinforcement.

$w(t = 0) = 7.5$ mm and a peak steel force of $N_s(t = 0) = 40.3$ kN. It can be seen that the normalized long-term amplifications of the deflection and reinforcement force due to creep are much larger than the ones obtained in Figure 5, due to the fact that the majority of the beam cross-section is under compression.

The dependence of the critical time to cause first creep rupture in compression on the level of the applied vertical load is shown in Figure 11. As expected, the critical time significantly decreases with the increase of the applied load. However, it is interesting to see that the logarithm of the critical time is almost linearly proportional to the level of the applied load. For $q_z < 0.7q_z^u$, no creep rupture is observed even 50 years after first loading. These observations are important for the design and the safety assessment of RC beams under high levels of sustained lateral and axial loadings, as creep may actually reduce the design life of such structures.

4.3. Comparison with test results. Only few detailed test results are available on the creep behavior of RC beams in general, and their nonlinear creep behavior in particular. Here, the test results reported in [Washa and Fluck 1952; Bakoss et al. 1982; Tan and Saha 2006] are used. Although the first two studies

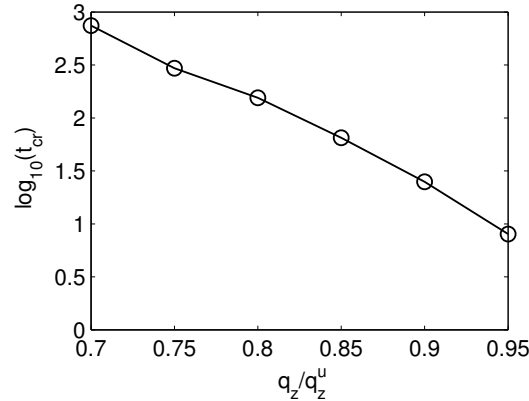


Figure 11. Variation of the critical time versus the initially applied vertical load.

focus on the creep behavior under linear stress levels, they provide a level of verification to the proposed model.

Bakoss et al. [1982] describe creep testing of a RC beam including experimental characterization of the creep and shrinkage material properties. The beam is simply supported with a span of 3504 mm, and is loaded in four points bending with sustained loads of 2.6 kN each applied at the third-points of the span. The beam has a rectangular cross section of 100/150 mm, and includes two 12 mm diameter deformed bars located at 20 mm from the bottom face of the beam. The reported compressive strength and modulus of elasticity are 39 MPa and 31.2 GPa, respectively, while following [CEB-FIP 1990], f_{ctm} and ε_c are taken as 3.47 MPa and -0.237% , respectively. The reported creep coefficient at $t = 560$ days and the shrinkage strain at $t = 775$ days that were measured from separate small specimens are 2.5 and -700×10^{-6} , respectively. It is assumed here that their development with time follows [CEB-FIP 1990]. Also here, seven Maxwell units are used with $T_\mu = 0.1 \times 5^{\mu-1}$ days, for $\mu = 1, \dots, 6$. For brevity, only the strain-independent parts of the spring moduli are reported here, as they are also the dominant parts due to the low level of sustained loading with linear stresses. Thus, $\bar{E}_\mu = [7.088 \ 2.132 \ 3.726 \ 3.947 \ 3.417 \ 2.877 \ 7.982]$ GPa.

Figure 12 shows the predicted and the measured time variation of the central deflection. Despite the unexpected sharp increase of the experimental deflection around $t = 250$ days, which can be due to environmental or other effects, the comparison reveals a reasonably good correlation between the results. The instantaneous deflection reported in the test is 8.94 mm, while the predicted one is 9.07 mm. The differences in the long-term deflections can be due to many factors including the different creep behavior of concrete in tension, compression, and bending, the use of a smeared cracking model, temperature and humidity changes, and other related factors.

Six beams (three pairs: A1, A4; A2, A5; and A3, A6) from the experimental investigation [Washa and Fluck 1952] are selected for the comparison. The beams were simply supported with a span of 6100 mm, and were loaded by concrete blocks to simulate a uniformly distributed load of 5.512 kN/m. All beams (A1–A6) have a rectangular cross section of 203/305 mm and include three bars of 19 mm diameter in tension. In addition, beams A2 and A5 include two 16 mm bars in compression, while beams A1 and A4 have symmetric reinforcement with three bars of 19 mm in compression. The reported

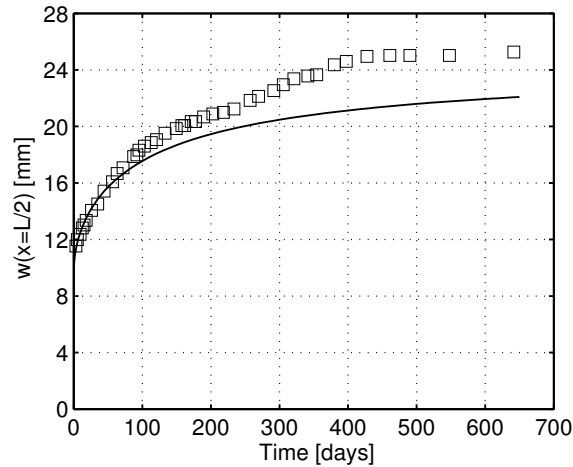


Figure 12. Theoretical versus experimental [Bakoss et al. 1982] results (the solid line is the proposed model and the squares the experimental results).

compressive strengths and moduli of elasticity vary between the different specimens in the range of $f_{ck} = 20.7\text{--}29.3$ MPa and $E_0 = 20.7\text{--}23.8$ GPa. For the numerical comparison, average values of $f_{ck} = 25.82$ MPa and $E_0 = 22.17$ GPa are chosen due to the low level of sustained loading where material nonlinearity has small influence. The creep coefficient and the shrinkage strain are estimated from the measured gross and net plastic flow in a cylinder prisms as 5 and -757×10^{-6} , respectively. Based on [CEB-FIP 1990], the following parameters are determined: $f_{ctm} = 3.15$ MPa and $\varepsilon_c = -0.218\%$. For brevity, only the strain-independent part of the spring moduli are reported with relaxation times taken as in the previous example. Thus, $\bar{E}_\mu = [7.44 \ 1.671 \ 2.945 \ 2.639 \ 2.046 \ 1.768 \ 3.63]$ GPa.

Table 1 shows the predicted w_{th} versus the measured w_{exp} instantaneous and long-term deflections 2.5 years after first loading. The experimental results are the average between the two similar beams. A good correlation between the results with a maximum difference of less than 16% can be observed. Additionally, it can be seen from the experimental results that the ratio between the long-term deflection and the instantaneous one significantly decreases with the addition of compressive reinforcement (2.63 for A3 and 1.75 for A1), as was discussed earlier (Figure 7). The predicted ratios are 3.18 for A3 and 1.57 for A1.

The experimental study reported in [Tan and Saha 2006] included testing of RC beams under high levels of sustained loads, that is, 70% and 80% of the ultimate load ($P_u = 26.8$ kN), which introduces a level of nonlinearity into the behavior. The beams were simply supported with a span of 1800 mm, and were symmetrically loaded by four point loads. The beams were 100/125 mm in cross-section and included

Beam	$w_{exp}(t=0)$	$w_{th}(t=0)$	$w_{exp}(t=2.5 \text{ years})$	$w_{th}(t=2.5 \text{ years})$
A1, A4	13.46	12.84	23.62	20.18
A2, A5	15.75	13.7	32.26	27.32
A3, A6	17	14.7	44.7	46.86

Table 1. Predicted versus measured [Washa and Fluck 1952] central deflection in mm.

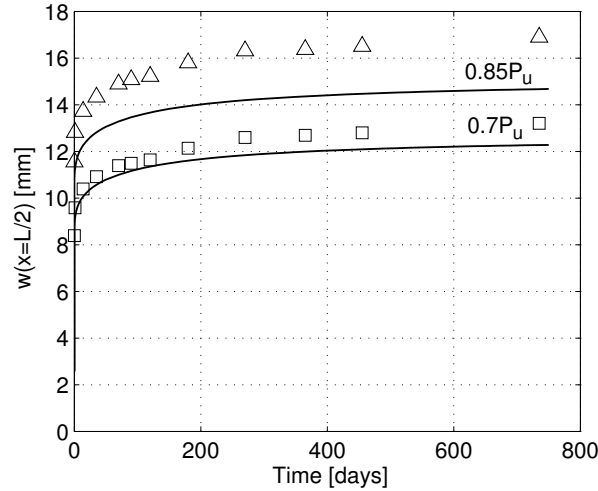


Figure 13. Theoretical versus experimental [Tan and Saha 2006] results (the solid line is the proposed model, the squares the experimental results under $0.7P_u$, and the triangles the experimental results under $0.85P_u$).

two bars of 10 mm diameter in tension and two bars of 6 mm in compression. The reported compressive strength, tensile strength, and modulus of elasticity are 40 MPa, 4.67 MPa, and 27.2 GPa, respectively, while ϵ_c was taken as -0.238%. The relaxation times were chosen as in the previous examples, while the spring moduli took the following strain-dependent form (in GPa) following (43):

$$\begin{bmatrix} \bar{E}_1 \\ \bar{E}_2 \\ \bar{E}_3 \\ \bar{E}_4 \\ \bar{E}_5 \\ \bar{E}_6 \\ \bar{E}_7 \end{bmatrix} = \begin{bmatrix} 5.094 & -7.642 & -5.382 & -2.307 & -3.649 \\ 1.677 & -1.719 & -1.211 & -0.519 & -0.82 \\ 2.98 & -2.847 & -2.005 & -0.859 & -1.36 \\ 3.365 & -1.896 & -1.335 & -0.572 & -0.904 \\ 3.098 & -0.742 & -0.522 & -0.223 & -0.356 \\ 2.358 & 0.134 & 0.943 & 0.396 & 0.652 \\ 8.607 & 4.311 & 3.036 & 1.302 & 2.058 \end{bmatrix} \begin{bmatrix} 1 \\ \epsilon_{xx}^v \\ (\epsilon_{xx}^v)^2 \\ (\epsilon_{xx}^v)^3 \\ (\epsilon_{xx}^v)^4 \end{bmatrix}. \quad (47)$$

The comparison between the theoretical and experimental results is shown in Figure 13, and reveals a reasonable agreement between the results (a maximum difference of less than 15%). It is not clearly seen in the figure, but the first day after loading is associated with a significant increase of the deflections of up to 14% of the instantaneous deflection, which is also predicted by the model. Additionally, the experimental observations confirm the results appearing in Figure 6 to some extent, where the ratio between the long-term deflection and the instantaneous one decreases with the increase of the level of the applied load (1.57 for $0.7P_u$ and 1.46 for $0.85P_u$).

5. Conclusions

The nonlinear creep response and the time-dependent cracking and creep rupture behavior of reinforced concrete (RC) beams have been discussed and investigated. A theoretical model has been developed,

which highlights the challenges associated with nonlinear creep modeling, and takes into account the effects of time-dependent cracking, creep rupture in compression, yielding of the reinforcement, shrinkage, and aging of the concrete material, via the nonlinear modified principle of superposition. The interaction between these parameters and their influence on the nonlinear creep response of RC beams have been highlighted through numerical and parametric studies.

The results have shown that due to the rapid release of the stresses after first loading, creep rupture in compression of flexural RC beams can rarely happen. However, with the existence of an axial compression force, creep rupture may dominate the structural behavior and reduce the load-carrying capacity of the member. In other words, under some circumstances, creep may continuously decrease the strength of RC beams. It has been shown that the critical time to cause creep rupture failure is very sensitive to the magnitude of the applied load, and it exponentially decreases with the increase of the load level. In addition, it has been observed that the amplifications due to creep of the deflection, curvature, and axial force in the reinforcement are different, and require detailed analysis for their assessment. Shrinkage and compressed reinforcement have been shown to play important roles in the long-term response, where the former tends to significantly increase the deformation and the cracked region, while the latter restrain these effects. A comparison with experimental results has been presented, which has revealed a reasonably good agreement between the results, and has provided a level of validation for the proposed model. Some of the test results observed in other studies have also been explained and clarified using the model.

Finally, it can be concluded that the nonlinear creep response of RC beams exhibits various physical phenomena that need to be fully understood and clarified. The analytical model developed in this paper explains some of these aspects, and provides a numerical tool and a theoretical basis for the nonlinear creep analysis of other RC members.

References

- [Bakoss et al. 1982] S. L. Bakoss, R. I. Gilbert, K. A. Faulkes, and V. A. Pilmano, “Long-term deflections of reinforced concrete beams”, *Mag. Concr. Res.* **34**:121 (1982), 203–212.
- [Bažant and Asghari 1977] Z. P. Bažant and A. A. Asghari, “Constitutive law for nonlinear creep of concrete”, *J. Eng. Mech. Div. (ASCE)* **103**:1 (1977), 113–124.
- [Bažant and Chern 1985] Z. P. Bažant and J.-C. Chern, “Strain softening with creep and exponential algorithm”, *J. Eng. Mech. (ASCE)* **111**:3 (1985), 391–415.
- [Bažant and Oh 1984] Z. P. Bažant and B. H. Oh, “Deformation of progressively cracking reinforced concrete beams”, *ACI J.* **81**:3 (1984), 268–278.
- [Bažant and Prasanna 1989] Z. P. a. Bažant and S. Prasanna, “Solidification theory for concrete creep, I: Formulation”, *J. Eng. Mech. (ASCE)* **115**:8 (1989), 1691–1703.
- [Bažant and Wu 1974] Z. P. Bažant and S. T. Wu, “Rate-type creep law of aging concrete based on Maxwell chain”, *Mater. Struct.* **7**:1 (1974), 45–60.
- [Bockhold and Petryna 2008] J. Bockhold and Y. Petryna, “Creep influence on buckling resistance of reinforced concrete shells”, *Comput. Struct.* **86**:7-8 (2008), 702–713.
- [Brueller and Steiner 1993] O. S. Brueller and H. Steiner, “Creep-based characterization of nonlinear relaxation behavior of plastics”, *Polym. Eng. Sci.* **33**:21 (1993), 1400–1403.
- [Carol and Bažant 1993] I. Carol and Z. P. Bažant, “Viscoelasticity with aging caused by solidification of nonaging constituent”, *J. Eng. Mech. (ASCE)* **119**:11 (1993), 2252–2269.

- [Carol and Murcia 1989] I. Carol and J. Murcia, "A model for the non-linear time-dependent behaviour of concrete in compression based on a Maxwell chain with exponential algorithm", *Mater. Struct.* **22**:3 (1989), 176–184.
- [CEB-FIP 1990] CEB-FIP, *Design Code*, Comité Euro-International du Béton, Thomas Telford House, London, 1990.
- [CEB-FIP 1999] CEB-FIP, *Structural concrete. Textbook on behaviour, design and performance. Updated knowledge of the CEB/FIP Model Code 1990*, Comité Euro-International du Béton/Fédération Internationale de la Précontrainte, Fib-bulletin no. 1, Lausanne, Switzerland, 1999.
- [Di Luzio 2009] G. Di Luzio, "Numerical model for time-dependent fracturing of concrete", *J. Eng. Mech. (ASCE)* **135**:7 (2009), 632–610.
- [Fernández Ruiz et al. 2007] M. Fernández Ruiz, A. Muttoni, and P. G. Gambarova, "Relationship between nonlinear creep and cracking of concrete under uniaxial compression", *J. Adv. Concr. Technol.* **5**:3 (2007), 383–393.
- [Findley et al. 1976] W. N. Findley, J. S. Lai, and K. Onran, *Creep and relaxation of nonlinear viscoelastic materials, with an introduction to linear viscoelasticity*, North-Holland, Amsterdam, 1976.
- [Gilbert 1988] R. I. Gilbert, *Time effects in concrete structures*, Elsevier, Amsterdam, 1988.
- [Gilbert 2007] R. I. Gilbert, "Tension stiffening in lightly reinforced concrete slabs", *J. Struct. Eng. (ASCE)* **133**:6 (2007), 899–903.
- [Hamed and Rabinovitch 2008] E. Hamed and O. Rabinovitch, "Nonlinear dynamic behavior of unreinforced masonry walls subjected to out-of-plane loads", *J. Struct. Eng. (ASCE)* **134**:11 (2008), 1743–1753.
- [Hamed et al. 2011] E. Hamed, M. A. Bradford, R. I. Gilbert, and Z. T. Chang, "Analytical model and experimental study of failure behavior of thin-walled shallow concrete domes", *J. Struct. Eng. (ASCE)* **137**:1 (2011), 88–99.
- [Leaderman 1943] H. Leaderman, *Elastic and creep properties of filamentous materials and other high polymers*, The Textile Foundation, Washington DC, 1943.
- [Li and Qian 1989] Z. Li and J. Qian, "Creep damage analysis and its application to nonlinear creep of reinforced concrete beam", *Eng. Fract. Mech.* **34**:4 (1989), 851–860.
- [Mazzotti and Savoia 2003] C. Mazzotti and M. Savoia, "Nonlinear creep damage model for concrete under uniaxial compression", *J. Eng. Mech. (ASCE)* **129**:9 (2003), 1065–1075.
- [Neville and Dilger 1970] A. M. Neville and W. H. Dilger, *Creep of concrete: plain, reinforced, and prestressed*, North-Holland, Amsterdam, 1970.
- [Omar et al. 2009] M. Omar, A. Loukili, G. Pijaudier-Cabot, and Y. Le Pape, "Creep-damage coupled effects: experimental investigation on bending beams with various sizes", *J. Mater. Civ. Eng. (ASCE)* **21**:2 (2009), 65–72.
- [Oza et al. 2003] A. Oza, R. Vanderby, and R. S. Lakes, "Interrelation of creep and relaxation for nonlinearly viscoelastic materials: application to ligament and metal", *Rheol. Acta* **42**:6 (2003), 557–568.
- [Papa et al. 1998] E. Papa, A. Taliercio, and E. Gobbi, "Triaxial creep behaviour of plain concrete at high stresses: a survey of theoretical models", *Mater. Struct.* **31**:7 (1998), 487–493.
- [Pipkin and Rogers 1968] A. Pipkin and T. Rogers, "A non-linear integral representation for viscoelastic behaviour", *J. Mech. Phys. Solids* **16**:1 (1968), 59–72.
- [Rabinovitch and Frostig 2001] O. Rabinovitch and Y. Frostig, "Nonlinear high-order analysis of cracked RC beams strengthened with FRP strips", *J. Struct. Eng. (ASCE)* **127** (2001), 381–389.
- [Rots and Blaauwendraad 1989] J. G. Rots and J. Blaauwendraad, "Crack models for concrete: discrete or smeared? fixed, multi-directional or rotating?", *Heron* **34**:1 (1989), 1–59.
- [Rots and de Borst 1987] J. G. Rots and R. de Borst, "Analysis of mixed-mode fracture in concrete", *J. Eng. Mech. (ASCE)* **113**:11 (1987), 1739–1758.
- [Santhikumar et al. 1998] S. Santhikumar, B. L. Karihaloo, and G. Reid, "A model for ageing visco-elastic tension softening material", *Mech. Cohes. Frict. Mater.* **3** (1998), 27–39.
- [Sorvari and Hämäläinen 2010] J. Sorvari and J. Hämäläinen, "Time integration in linear viscoelasticity: a comparative study", *Mech. Time-Depend. Mater.* **14**:3 (2010), 307–328.
- [Stoer and Bulirsch 2002] J. Stoer and R. Bulirsch, *Introduction to numerical analysis*, Springer, 2002.

- [Tan and Saha 2006] K. H. Tan and M. K. Saha, “Long-term deflections of reinforced concrete beams externally bonded with FRP system”, *J. Compos. Constr. (ASCE)* **10**:6 (2006), 474–482.
- [Taylor et al. 1970] R. Taylor, K. Pister, and G. Goudreau, “Thermomechanical analysis of viscoelastic solids”, *Int. J. Numer. Methods Eng.* **2**:1 (1970), 45–59.
- [Touati and Cederbaum 1997] D. Touati and G. Cederbaum, “Stress relaxation of nonlinear thermoviscoelastic materials predicted from known creep”, *Mech. Time-Depend. Mater.* **1**:3 (1997), 321–330.
- [Washa and Fluck 1952] G. W. Washa and P. G. Fluck, “Effect of compressive reinforcement on the plastic flow of reinforced concrete beams”, *ACI J.* **49**:10 (1952), 89–108.
- [Zhou 1994] F. P. Zhou, “Numerical modelling of creep crack growth and fracture in concrete”, pp. 141–148 in *Localized damage III: computer-aided assessment and control*, edited by M. H. Aliabadi et al., Transactions on Engineering Sciences **6**, WIT Press, Ashurst Lodge, Southampton, 1994.

Received 24 Nov 2011. Revised 9 Feb 2012. Accepted 21 Feb 2012.

EHAB HAMED: e.hamed@unsw.edu.au

Centre for Infrastructure Engineering and Safety, The School of Civil and Environmental Engineering,
The University of New South Wales, Sydney, NSW 2052, Australia

JOURNAL OF MECHANICS OF MATERIALS AND STRUCTURES

jomms.net

Founded by Charles R. Steele and Marie-Louise Steele

EDITORS

CHARLES R. STEELE Stanford University, USA
DAVIDE BIGONI University of Trento, Italy
IWONA JASIUK University of Illinois at Urbana-Champaign, USA
YASUhide SHINDO Tohoku University, Japan

EDITORIAL BOARD

H. D. BUI École Polytechnique, France
J. P. CARTER University of Sydney, Australia
R. M. CHRISTENSEN Stanford University, USA
G. M. L. GLADWELL University of Waterloo, Canada
D. H. HODGES Georgia Institute of Technology, USA
J. HUTCHINSON Harvard University, USA
C. HWU National Cheng Kung University, Taiwan
B. L. KARIHALOO University of Wales, UK
Y. Y. KIM Seoul National University, Republic of Korea
Z. MROZ Academy of Science, Poland
D. PAMPLONA Universidade Católica do Rio de Janeiro, Brazil
M. B. RUBIN Technion, Haifa, Israel
A. N. SHUPIKOV Ukrainian Academy of Sciences, Ukraine
T. TARNAI University Budapest, Hungary
F. Y. M. WAN University of California, Irvine, USA
P. WRIGGERS Universität Hannover, Germany
W. YANG Tsinghua University, China
F. ZIEGLER Technische Universität Wien, Austria

PRODUCTION contact@msp.org

SILVIO LEVY Scientific Editor

Cover design: Alex Scorpan

Cover photo: Wikimedia Commons

See <http://jomms.net> for submission guidelines.

JoMMS (ISSN 1559-3959) is published in 10 issues a year. The subscription price for 2012 is US \$555/year for the electronic version, and \$735/year (+\$60 shipping outside the US) for print and electronic. Subscriptions, requests for back issues, and changes of address should be sent to Mathematical Sciences Publishers, Department of Mathematics, University of California, Berkeley, CA 94720–3840.

JoMMS peer-review and production is managed by EditFLOW[®] from Mathematical Sciences Publishers.

PUBLISHED BY
 **mathematical sciences publishers**
<http://msp.org/>

A NON-PROFIT CORPORATION

Typeset in L^AT_EX

Copyright ©2012 by Mathematical Sciences Publishers

Journal of Mechanics of Materials and Structures

Volume 7, No. 5

May 2012

Scale effects on ultrasonic wave dispersion characteristics of monolayer graphene embedded in an elastic medium

SAGGAM NARENDAR and SRINIVASAN GOPALAKRISHNAN 413

Nonlinear creep response of reinforced concrete beams **EHAB HAMED 435**

New invariants in the mechanics of deformable solids

VIKTOR V. KUZNETSOV and STANISLAV V. LEVYAKOV 461

Two cases of rapid contact on an elastic half-space: Sliding ellipsoidal die, rolling sphere

LOUIS MILTON BROCK 469

Buckling analysis of nonuniform columns with elastic end restraints

SEVAL PINARBASI 485



1559-3959(2012)7:5;1-9